*molecules*

MDPI

*Article*

# Synthesis, Experimental and Theoretical Study of Azidochromones

**Ena G. Narváez-Ordoñez [1], Kevin A. Pabón-Carcelén [1], Daniel A. Zurita-Saltos [1], Pablo M. Bonilla-Valladares [1], Trosky G. Yánez-Darquea [1], Luis A. Ramos-Guerrero [2], Sonia E. Ulic [3,4], Jorge L. Jios [5], Gustavo A. Echeverría [6], Oscar E. Piro [6], Peter Langer [7,8], Christian D. Alcívar-León [1,*] and Jorge Heredia-Moya [9,*]**

1 Facultad de Ciencias Químicas, Universidad Central del Ecuador, Francisco Viteri s/n y Gilberto Gato Sobral, Quito 170521, Ecuador; egnarvaezo@uce.edu.ec (E.G.N.-O.); kevincarcelen@outlook.com (K.A.P.-C.); dazuritas@uce.edu.ec (D.A.Z.-S.); pmbonilla@uce.edu.ec (P.M.B.-V.); tgyanez@uce.edu.ec (T.G.Y.-D.)
2 Centro de Investigación de Alimentos CIAL, Universidad UTE, Quito 170527, Ecuador; luis.ramos@ute.edu.ec
3 CEQUINOR (CONICET-UNLP), Facultad de Ciencias Exactas, Universidad Nacional de La Plata, Bv. 120 No 1465, La Plata 1900, Buenos Aires, Argentina; sonia@quimica.unlp.edu.ar
4 Departamento de Ciencias Básicas, Facultad de Ciencias Exactas, Universidad Nacional de Luján, Rutas 5 y 7, Luján 6700, Buenos Aires, Argentina
5 Laboratorio UPL (UNLP-CIC), Camino Centenario e/505 y 508 (1897) M.B. Gonnet and Departamento de Química, Facultad de Ciencias Exactas, Universidad Nacional de La Plata, República Argentina. 47 esq. 115, La Plata 1900, Buenos Aires, Argentina; jljios@quimica.unlp.edu.ar
6 Departamento de Física, Facultad de Ciencias Exactas, Universidad Nacional de La Plata e IFLP (CONICET, CCT-La Plata), La Plata 1900, Buenos Aires, Argentina; geche@fisica.unlp.edu.ar (G.A.E.); piro@fisica.unlp.edu.ar (O.E.P.)
7 Institut für Chemie, Universität Rostock, Albert-Einstein-Str. 3a, 18059 Rostock, Germany; peter.langer@uni-rostock.de
8 Leibniz Institut für Katalyse, Universität Rostock e. V. (LIKAT), Albert-Einstein-Str. 29a, 18059 Rostock, Germany
9 Centro de Investigación Biomédica (CENBIO), Facultad de Ciencias de la Salud Eugenio Espejo, Universidad UTE, Quito 170527, Ecuador
* Correspondence: cdalcivar@uce.edu.ec (C.D.A.-L.); jorgeh.heredia@ute.edu.ec (J.H.-M.)

**Abstract:** A series of 2-(haloalkyl)-3-azidomethyl and 6-azido chromones has been synthetized, characterized and studied by theoretical (DFT calculations) and spectroscopic methods (UV-Vis, NMR). The crystal structure of 3-azidomethyl-2-difluoromethyl chromone, determined by X-ray diffraction methods, shows a planar framework due to extended π-bond delocalization. Its molecular packing is stabilized by F···H, N···H and O···H hydrogen bonds, π···π stacking and C–O···π intermolecular interactions. Moreover, AIM, NCI and Hirshfeld analysis evidenced that azido moiety has a significant role in the stabilization of crystal packing through weak intermolecular interactions, where analysis of electronic density suggested closed-shell (CS) interatomic interactions.

**Keywords:** azidochromone; spectroscopic properties; structural X-ray diffraction; quantum chemical calculations; Hirshfeld surface analysis

check for updates

**Citation:** Narváez-Ordoñez, E.G.; Pabón-Carcelén, K.A.; Zurita-Saltos, D.A.; Bonilla-Valladares, P.M.; Yánez-Darquea, T.G.; Ramos-Guerrero, L.A.; Ulic, S.E.; Jios, J.L.; Echeverría, G.A.; Piro, O.E.; et al. Synthesis, Experimental and Theoretical Study of Azidochromones. *Molecules* **2022**, *27*, 2636. https://doi.org/10.3390/molecules27092636

Academic Editors: Philippe Belmont, Wim Dehaen and Eugene Babaev

Received: 31 January 2022
Accepted: 16 February 2022
Published: 20 April 2022

**Publisher's Note:** MDPI stays neutral with regard to jurisdictional claims in published maps and institutional affiliations.



## 1. Introduction

Chromone derivatives with reactive functional groups such as halogens [1,2], haloalkyl [3–5], hydroxyl [6], amino [7,8] and azide [8,9] are important cores and precursors for pharmacologically active compounds (anti-cancer, anti-HIV, antioxidant, anti-tubercular, anti-inflammatory, analgesic, antimicrobial, anti-malaria, gastroprotective, antihistamine and antihypertensive) [10–14]. Among them, haloalkyl groups and azides are particularly relevant, both for their accessible synthetic routes and for their wide use as precursors of reactive species [15]. Nitrenes and nitrenium ions can be generated from azides, which

also serve as anchors for synthesis of nitrogen-rich compounds such as aziridines, azirines, triazoles, triazolines and triazides [9,15].

Different 2-trifluoromethyl and 2-(polyfluoroalkyl)chromones have been studied extensively [16–19]. Despite their ready accessibility, these compounds have been ignored by synthetic chemists, although their systematic study has been revitalized in recent years. The main basic structure of chromones serves as a scaffold for novel compounds with biological importance, improving their solubility and pharmacokinetic properties [20–22]. In addition, the presence of electron-withdrawing polyfluoroalkyl groups attached to the C-2 carbon of chromones crucially modifies the reactivity and electron-density distribution around the α,β-unsaturated carbonyl portion of the pyrone ring [23]. These changes expand the synthetic potential of 3-substituted-2-polyfluoroalkylchromones, their structural study being our area of interest in this research.

This work reports the synthesis, characterization and computational study of five novel halo-chromones (Scheme 1, Scheme S1 and Table S1, Supplementary Materials) with the azido group.

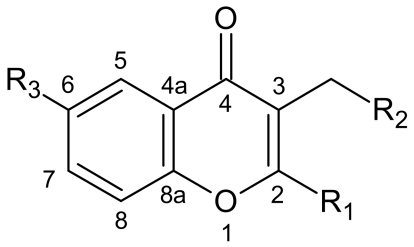


| Product | $R_1$ | $R_2$ | $R_3$ |
|---|---|---|---|
| **1** | $–CF_2Cl$ | $–N_3$ | –H |
| **2** | $–CF_3$ | –H | $–N_3$ |
| **3** | $–CF_3$ | $–N_3$ | –H |
| **4** | $–CF_2H$ | $–N_3$ | –H |
| **5** | $–CF_2CF_3$ | $–N_3$ | –H |

**Scheme 1.** Azidochromones.

## 2. Results and Discussion

### *2.1. Conformational Analysis*

Geometries of compounds **1–5** in the gas phase were studied, determined and calculated through a conformational analysis using the B3LYP/6-311++G(d,p) level of theory. Potential energy curves were performed by torsions around the C2–C2′ and C3–C3′ bonds that connect both exocyclic carbons C2′ (bearing the halogen atoms) and C3′ with the corresponding C2 and C3 carbon atoms of the heterocyclic ring C2 and C3, respectively. The most stable conformations of **1–5** and the main parameters are presented in Table 1 (See Figures S1–S4, Supplementary Materials).

**Table 1.** Structural parameters, dihedral angles and populations of the theoretical conformations for **1–5**.

| Compound | Conformation | $\phi$ (C2-C3-C3′-X) [a,c] | $\phi$ (C3-C2-C2′-Y) [b,c] | % Population |
|---|---|---|---|---|
| **1** | **1 a** | 95 (ac) [c] | 94 (ac) | 51 |
| | **1 b** | −81 (−sc) | 106 (ac) | 26 |
| | **1 c** | −102 (−ac) | 82 (sc) | 13 |
| | **1 d** | −66 (−sc) | 104 (ac) | 10 |
| **2** | **2** | 102 (ac) | −55 (−sc) | 100 |
| **3** | **3 a** | 88 (sc) | −8 (sp) | 66 |
| | **3 b** | 101 (ac) | 31 (sc) | 34 |
| **4** | **4 a** | 64 (sc) | 113 (ac) | 84 |
| | **4 b** | −105 (−ac) | −62 (−sc) | 16 |
| **5** | **5 a** | 98 (ac) | 90 (sc) | 67 |
| | **5 b** | 107 (ac) | −87 (−sc) | 17 |
| | **5 c** | 102 (ac) | −175 (−ap) | 16 |

[a] X = H, N; [b] Y = F, Cl; [c] sp: synperiplanar, sc: synclinal, ac: anticlinal, ap: antiperiplanar.

### 2.2. NMR Spectroscopy

Experimental chemical shifts were compared with those derived from chemical calculations using the B3LYP/6-311+G(2d,p) level of theory (Table 2). For protons, a good agreement is observed with $\Delta = TM_{exp} - TM_{calc}$ deviation ranging from −0.49 to 0.27 ppm, except for the $CH_2N_3$ of **1** ($\Delta = -0.74$). For carbon, the deviation range is between −32.2 and 10.9 ppm. The linear relationship between computed and experimental data, for all compounds, gives R-square values above 0.978 and 0.945 for protons (see Figure S5, Supplementary Materials) and carbons, respectively. The highest deviation was found for $CF_2Cl$ and $CF_3$ of **1** and **2** with Δ values of −32.2 and −22.1 ppm, respectively; this suggests that the isotropic shielding of the fluorine atoms is underestimated by theoretical calculations, as previously reported [24–27]. Analysis of signal multiplicity and coupling constants was used, in conjunction with the calculated data, for structural elucidation.

**Table 2.** Comparison between experimental and calculated chemical shifts (ppm) of $^1$H and $^{13}$C-NMR spectra of compounds **1–5**.

| | **1** | | | **2** | | | **3** | | | **4** | | | **5** | | |
|---|---|---|---|---|---|---|---|---|---|---|---|---|---|---|---|
| **Atom** | **Exp.** | **Calc.** | **(Δ)** | **Exp.** | **Calc.** | **Δ** | **Exp.** | **Calc.** | **Δ** | **Exp.** | **Calc.** | **Δ** | **Exp.** | **Calc.** | **Δ** |
| $CH_3$ | — | — | — | 2.25 | 1.98 | 0.27 | — | — | — | — | — | — | — | — | — |
| $CH_2N_3$ | 4.53 | 5.27 | −0.74 | — | — | — | 4.46 | 4.51 | −0.05 | 4.50 | 4.44 | 0.06 | 4.46 | 4.51 | −0.05 |
| $CHF_2$ | — | — | — | — | — | — | — | — | — | 7.09 | 7.10 | −0.01 | — | — | — |
| H-5 | 8.27 | 8.59 | −0.32 | 8.19 | 7.98 | 0.21 | 8.25 | 8.66 | −0.41 | 8.18 | 8.67 | −0.49 | 8.26 | 8.67 | −0.41 |
| H-6 | 7.53 | 7.56 | −0.03 | — | — | — | 7.50 | 7.70 | −0.2 | 7.55 | 7.67 | −0.12 | 7.56 | 7.70 | −0.14 |
| H-7 | 7.82 | 7.85 | −0.03 | 7.69 | 7.58 | 0.11 | 7.79 | 7.94 | −0.15 | 7.87 | 7.97 | −0.10 | 7.80 | 7.99 | −0.19 |
| H-8 | 7.59 | 7.57 | 0.02 | 7.49 | 7.39 | 0.10 | 7.55 | 7.71 | −0.16 | 7.66 | 7.82 | −0.16 | 7.50 | 7.70 | −0.20 |
| C-2 | 154.5 | 161.0 | −6.5 | 148.5 | 155.0 | −6.5 | 151.0 | 157.7 | −6.7 | 157.2 | 163.8 | −6.6 | 150.5 | 156.5 | −6.0 |
| C-3 | 118.4 | 127.0 | −8.6 | 134.9 | 124.0 | 10.9 | 119.0 | 127.8 | −8.8 | 119.8 | 125.6 | −5.8 | 121.5 | 132.5 | −11.0 |
| C-4 | 177.1 | 188.0 | −10.9 | 176.8 | 186.0 | −9.2 | 176.9 | 182.0 | −5.1 | 178.7 | 180.2 | −1.5 | 176.8 | 182.0 | −5.2 |
| C-4a | 122.6 | 128.0 | −5.4 | 131.9 | 128.0 | 3. | 122.9 | 128.6 | −5.7 | 124.0 | 129.5 | −5.5 | 122.7 | 128.9 | −6.2 |
| C-5 | 126.6 | 131.0 | −4.4 | 119.9 | 133.0 | −13.1 | 126.4 | 132.7 | −6.3 | 127.5 | 132.5 | −5.0 | 126.9 | 132.5 | −5.6 |
| C-6 | 126.3 | 126.0 | 0.3 | 136.0 | 129.0 | 7.0 | 126.8 | 130.7 | −3.9 | 126.7 | 131.4 | −4.7 | 126.5 | 130.4 | −3.9 |
| C-7 | 135.3 | 140.0 | −4.7 | 125.4 | 128.0 | −2.6 | 135.5 | 139.6 | −4.1 | 136.6 | 139.7 | −3.1 | 135.5 | 139.1 | −3.6 |
| C-8 | 116.8 | 121.0 | −4.2 | 123.2 | 123.0 | 0.2 | 118.5 | 122.1 | −3.6 | 119.6 | 122.6 | −3.0 | 118.4 | 121.6 | −3.2 |
| C-8a | 154.9 | 164.0 | −9.1 | 153.3 | 161.0 | −7.7 | 155.2 | 162.0 | −6.8 | 157.0 | 162.5 | −5.5 | 155.4 | 162.2 | −6.8 |
| $CH_3$ | — | — | — | 8.7 | 11.4 | −2.7 | — | — | — | — | — | — | — | — | — |
| $CH_2N_3$ | 42.8 | 45.5 | −2.70 | — | — | — | 42.8 | 45.6 | −2.8 | 43.3 | 44.4 | −1.1 | 42.9 | 48.4 | −5.5 |
| $CF_2Cl$ | 120.8 | 153.0 | −32.2 | — | — | — | — | — | — | — | — | — | — | — | — |
| $CF_3$ | — | — | — | 120.9 | 143.0 | −22.1 | 119.4 | 131.4 | −12.0 | — | — | — | — | — | — |
| $CF_2H$ | — | — | — | — | — | — | — | — | — | 111.0 | 117.0 | −6.0 | — | — | — |
| $CF_2CF_3$ | — | — | — | — | — | — | — | — | — | — | — | — | — | 120.0 | — |
| $CF_2CF_3$ | — | — | — | — | — | — | — | — | — | — | — | — | — | 129.9 | — |

### 2.3. Electronic Spectra

The calculated and experimental (using methanol as solvent (**1**: $1.05 \times 10^{-5}$ M, **2**: $1.25 \times 10^{-4}$ M, **3**: $1.05 \times 10^{-5}$ M, **4**: $1.99 \times 10^{-5}$ M, **5**: $2.51 \times 10^{-5}$ M)) electronic absorption spectra (see Figures S6–S10, Supplementary Materials) of **1–5** are shown in Table 3. Electronic spectra were calculated at the TD-B3LYP/6-311++G(d,p) level of theory, implicitly considering the influence of the solvent (methanol, ε = 32.7), with the conductor-like polar-

izable continuum model (CPCM). The main experimental absorption bands were correlated with the calculated vertical electronic transitions, with oscillator strengths (f) > 0.076.

**Table 3.** Experimental and calculated (B3LYP/6-311++G(d,p) electronic spectra of **1**–**5**.

| Compound | Experimental [a] | Calculated [b] | Assignment |
|---|---|---|---|
| **1** | 204 (4.62) | 211 (0.177) | HOMO − 1 → LUMO + 3 (51%) |
| | 225 (4.42) | 237 (0.136) | HOMO − 5 → LUMO (49%) |
| | 244 (4.23) | 289 (0.121) | HOMO − 2 → LUMO (88%) |
| | 303 (4.00) | 330 (0.076) | HOMO → LUMO (74%) |
| **2** | 203 (3.87) | 212 (0.228) | HOMO → LUMO + 5 (25%) |
| | 230 (3.81) | 271 (0.599) | HOMO − 2 → LUMO (41%) |
| | 318 (3.24) | 361 (0.116) | HOMO → LUMO (88%) |
| **3** | 204 (4.55) | 201 (0.185) | HOMO – 2 →LUMO + 2 (43%) |
| | 223 [c] (4.34) | 223 (0.103) | HOMO – 5 → LUMO + 1 (50%) |
| | 250 [c] (4.06) | 250 (0.230) | HOMO → LUMO + 1(37%) |
| | 305 (3.95) | 304 (0.091) | HOMO → LUMO (95%) |
| **4** | 204 (4.63) | 204 (0.306) | HOMO – 2 → LUMO + 2 (44%) |
| | 224 (4.56) | 233 (0.140) | HOMO → LUMO + 2 (37%) |
| | | | HOMO – 4 → LUMO (32%) |
| | 246 [c] (4.36) | 250 (0.210) | HOMO → LUMO + 1 (64%) |
| | 301 (4.14) | 300 (0.093) | HOMO → LUMO (80%) |
| **5** | 204 (4.65) | 203 (0.202) | HOMO – 2 → LUMO + 2 (50%) |
| | 221 (4.46) | 223 (0.079) | HOMO – 5 → LUMO (59%) |
| | 246 (4.35) | 238 (0.108) | HOMO – 4 → LUMO (72%) |
| | | 249 (0.233) | HOMO → LUMO + 1 (65%) |
| | | 271 (0.084) | HOMO – 2 → LUMO (75%) |
| | 304 (4.12) | 305 (0.108) | HOMO → LUMO (82%) |

[a] In nm and log$\varepsilon$ (in parentheses). [b] In nm and oscillator strength (in parentheses) in a.u. [c] Shoulder.

The main molecular orbitals, involved in the electronic transitions of **1**–**5**, are depicted in Figures S11–S13 (Supplementary Materials).

The most intense absorption band of **1**, localized at 204 nm (calc. 211 nm), is attributed to HOMO − 1 → LUMO + 3 transitions principally due to excitations from $\pi$-bonding orbitals of the aromatic ring and non-bonding orbitals of N1 and N3 atoms to $\pi$*-orbitals of the benzene ring and p-type orbitals of one fluorine atom.

The strong bands at 203 nm for **2** and 204 nm for **3**–**5** derive from electronic excitations from HOMO → LUMO + 5 (**2**) and HOMO − 2 → LUMO + 2 (**3**–**5**). The absorption at 203 nm (calc. 212 nm) arises from principally $\pi$-bonding orbitals of the aromatic ring and nitrogen atoms (N1 and N3) non-bonding orbitals of the azide moiety to $\pi$*-orbitals delocalized along the whole molecule.

The absorption at 204 nm (**3**–**5**) is originated in all cases from $\pi \rightarrow \pi^*$ transitions within the aromatic ring and to $\pi$*-orbitals of C=C and N2=N3 bonds.

The dominant HOMO → LUMO excitation for **1**–**5** was assigned to the observed bands at 303, 318, 305, 301 and 304 nm, respectively. This absorption is mainly generated by transitions from $\pi$-orbitals of the aromatic ring and C=C bonds and with the contribution of non-bonding orbitals of both oxygen, N1 and N3 atoms to $\pi$*-orbitals of the benzene ring and p-type orbitals of some carbon atoms of the heterocycle.

### *2.4. Crystallographic Structural Results of (**4**) or: Crystal Structure of **4***

Figure 1 is an ORTEP [28] drawing of the molecule, and its bond distances and angles are presented in Tables S2–S5 (Supplementary Materials).

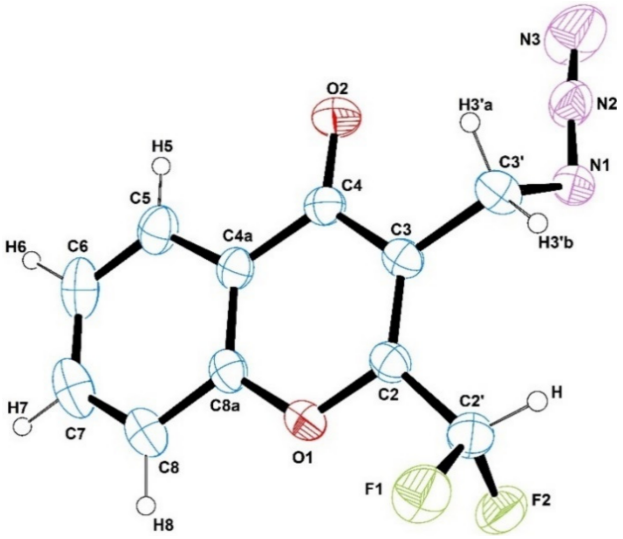


**Figure 1.** ORTEP plot of chromone **4** showing the labeling of the non-H atoms and their displacement ellipsoids at the 30% probability level.

Due to extended π-bonding, the chromone molecular skeleton is planar (rms deviation of atoms from the best least-squares plane is 0.043 Å). Observed bond distances and angles agree with established organic chemistry rules. In fact, phenyl ring C–C distances [from 1.363(3) to 1.398(3) Å] are as expected for a resonant-bond structure. The fused heterocycle shows a C2–C3 bond length of 1.339(3) Å, shorter than the other heterocycle C–C distances [from 1.381(3) to 1.468(3) Å], which corresponds formally to double-bond character for that link. Heterocycle C–O single-bond distances are 1.355(2) Å and 1.375(2) Å, and the carbonyl C=O double-bond length is equal to 1.227(2) Å. The molecular metrics of the chromone skeleton agree with one of the corresponding closely related chromone derivatives [5,24,25]. The $–C_{(sp3)}F_2H$ and $–C_{(sp3)}H_2(N_3)$ groups exhibit the expected tetrahedral bonding structure. C–C–F angles are 108.1(2)° and 110.3(2)° and the F–C–F angle is 106.0(2)°. The C–C–$N_3$ bond angle is 111.23° and ∠ (C–N=N2) = 114.5(2)°. The observed C–F bond distances are 1.351(2) and 1.363(3) Å and d(C–N3) = 1.478(3) Å. Azide N=N bond lengths are 1.221(2) Å (bonded to the carbon end) and 1.126(3) Å.

### *2.5. Hirshfeld Surface Analysis*

Figure 2a shows the crystal packing of **4** stabilized by $R_2^2(14)$, $R_4^4(8)$, $R_2^2(10)$, $R_4^4(8)$ and $R_2^2(13)$ graph-set ring motifs, which form dimers and tetramers in the supramolecular assembly. The F1 and F2 fluorine atoms of the $–CF_2H$ moiety interact individually with an aromatic and an aliphatic hydrogen atom, forming $C7_{(sp2)}$–H7···F2 and $C3'_{(sp3)}$–H3′···F1 intermolecular contacts along the c-axis. Moreover, the $C7_{(sp2)}$–H7···F2 angle is nearly linear (173°), while the observed angle for $C3'_{(sp3)}$–H3′···F1 (107°) reveals a moderate angular directionality. In this sense, the d(H7···F2) intermolecular distance (2.540 Å) is shorter than that observed in 3-bromomethyl-2-trifluoromethylchromone [3] and $CF_3/CF_2H$-substituted benzene, where the role of $CF_3/CF_2H$ groups in the C–H···F intermolecular interactions contributes significantly to the stability and molecular arrangement of the crystal structures (see Table S6, Supplementary Materials). While the $C2'_{(sp3)}$–H···O2, $C5_{(sp2)}$–H5···N1, $C2'_{(sp3)}$–F1···N2 and $C2'_{(sp3)}$–F2···N3 contacts could be considered weak intermolecular interactions due to their directionality and length [29], the azide ($N_3$), carbonyl and $CF_2H$ groups play a significant role in crystal packing. This becomes evident by the relative

contribution percentage of the intermolecular contacts, the character and their interaction energies evaluated with the Hirshfeld Surface, AIM and NCI analysis (see below).

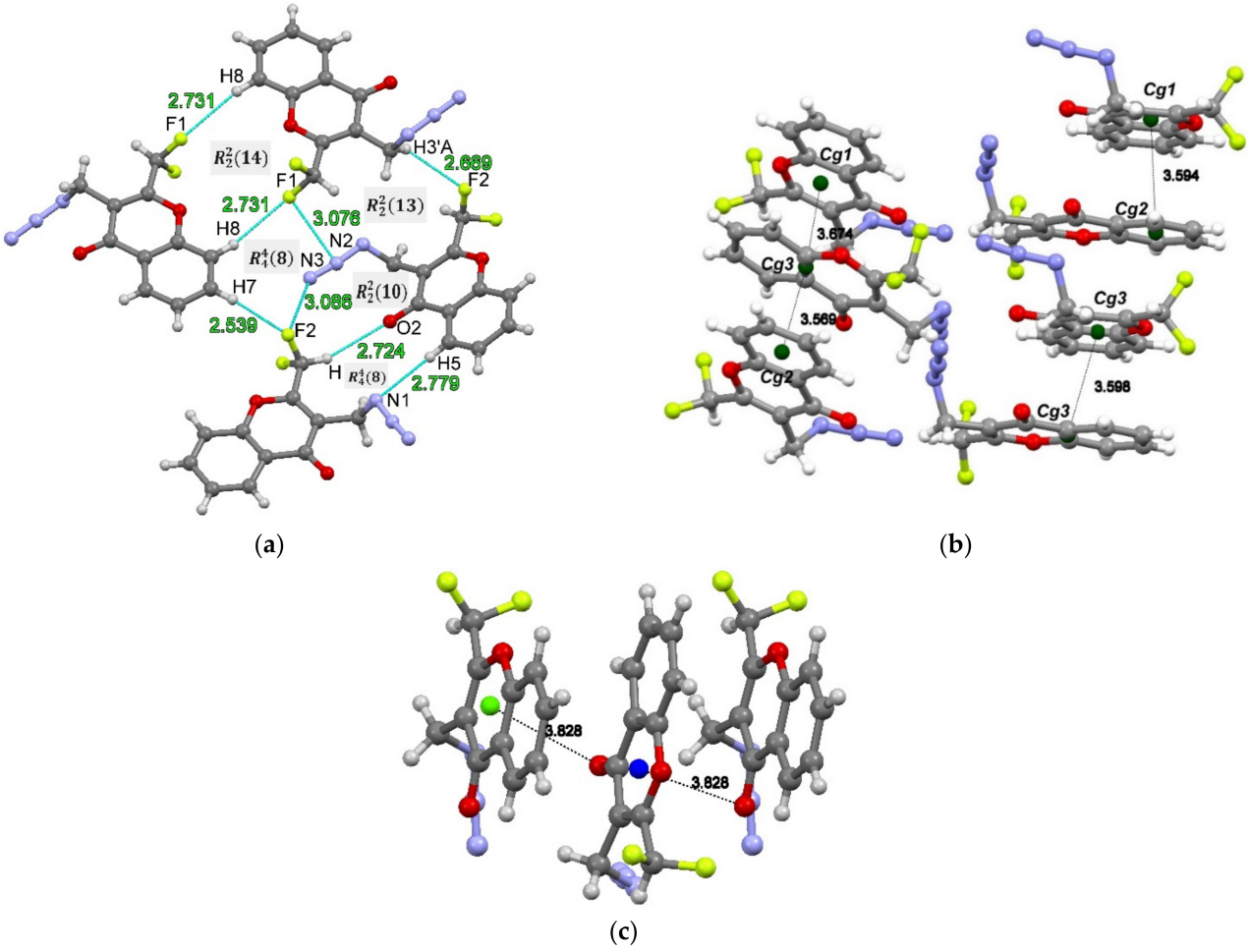


**Figure 2.** (**a**) Packing diagram of **4** via $C_{sp2}$–H···F–$C_{sp3}$ and $C_{sp3}$–H···F–$C_{sp3}$ intermolecular interactions (dotted lines). (**b**) A view of the π···π stacking intercentroids distances of **4**. (**c**) A view of C–O···π stacking (dashed lines) for compound **4**.

Intramolecular π-stacking contacts (Figure 2b) are observed between the chromone ring (Cg1···Cg3, distances of 3.674 Å and Cg2···Cg3, distances of 3.569 Å) and the benzene moiety, and intramolecular offset-face-to-face π-stacking contacts between the benzene moiety and 4-pyrone ring (Cg1···Cg2, distances of 3.594 Å). Moreover, short distances for π-stacking contacts between the chromone rings (Cg3···Cg3, distances of 3.674 Å) and π···π arrangements in **4** show short distances of contact (Table S7, Supplementary Materials) compared with chromone derivatives substituted in 3, 5 and 7 positions [30], where the linear stacking of forces π···π can be considered the agent that influences the strengthening of the molecular assembly. Additionally, Figure 2c shows C–O···π contacts between the carbonyl group and 4-pyrone ring. The oxygen atom of the carbonyl group in the C-O···π intermolecular interactions (Table S8, Supplementary Materials) behaves similar to interactions observed in N-arylamides, where the interactions evidence a stronger electrostatic character [31].

To explore the features associated with the role of intermolecular contacts, a Hirshfeld surface analysis of **4** was performed (Figures 3 and 4) [32]. Figure 3a evidences contacts shorter than van der Waals, as highlighted by the red dots on the $d_{norm}$ surface, where the hydrogen and fluorine atoms of the $–CH_2N_3$, $–CF_2H$ and $–C_{Ar}–H$ moieties promote intermolecular contacts. In this sense, Tables S9 and S10 and Figure S14 (Supplementary Ma-

terials) show the crystal lattice energy calculated with the CE-B3LYP/6− 31 G(d,p) energy model; for the C–H···F contacts, a character significative of contribution-dispersive ($E_{dis.}$) and -repulsive interaction ($E_{rep.}$) energies was observed. Particularly, the C3′-H3′A···F2 intermolecular contact displayed an important contribution with a relative high impact of dispersive, repulsive and total energy of −23.4 kcal/mol, 12.9 kcal/mol and −21.2 kcal/mol, respectively. The interactions' energy results are in agreement with those observed in 3-dibromomethyl-2-difluoromethylchromone [5]. Moreover, shape index and curvedness properties evidence π···π stacking and C–O···π interactions [33], which arise from planar stacking arrangements between the chromone rings. Features such as 'bow-tie' patterns of large red and blue triangles (see red circle in Figure 3b) and large green flat regions delineated by a blue outline (Figure 3c) reveal these close contacts associated with weak interactions [30].

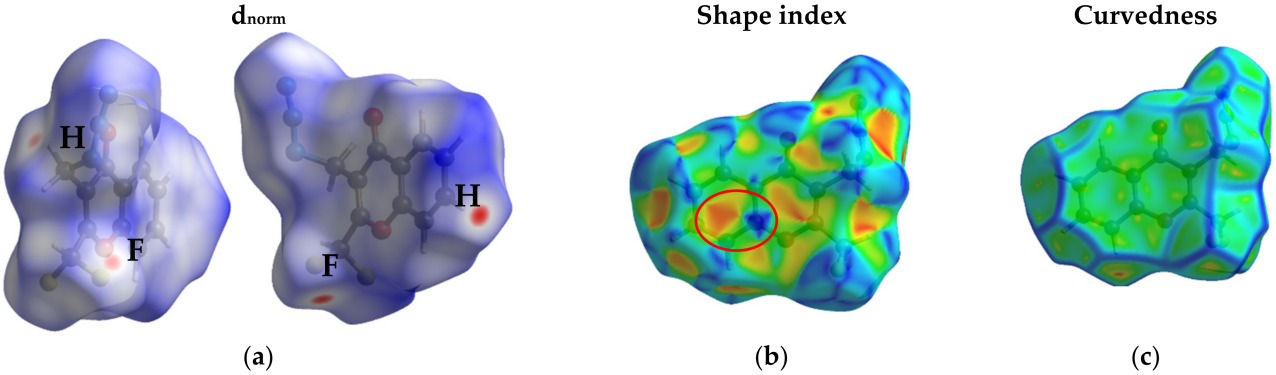


**Figure 3.** Hirshfeld surfaces mapped over $d_{norm}$ (**a**), shape index (**b**) and curvedness index of **4** (**c**).

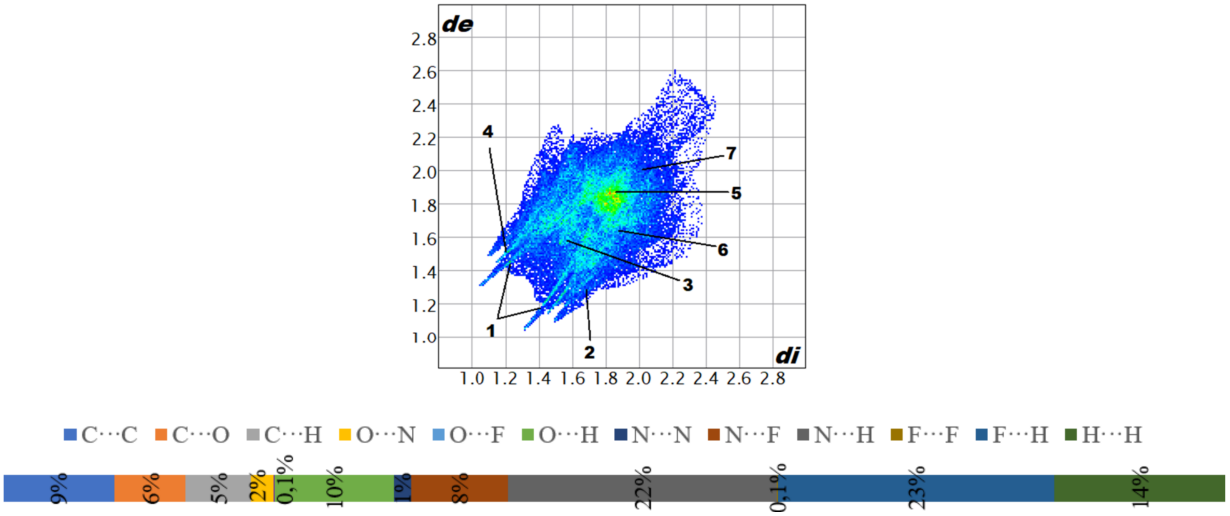


**Figure 4.** Top: 2D-fingerprint plot of **4**. Close contacts are labeled as 1: F···H (23%), 2: N···H (22%), 3: H···H (14%), 4: O···H (10%), 5: C···C (9%), 6: N···F (8%), 7: C···O (6%). Bottom: Relative contribution (%) of intermolecular contacts to the Hirshfeld surface area of **4**.

Figure 4 shows the 2D-fingerprint plot of the main intermolecular contacts of **4**. The pair of narrow spikes, labeled 1, corresponds to the shortest F···H distance associated to C–H···F interactions, while 2 evidences the N···H contacts that arise from C5–H5···N1 interactions. The F···H and N···H contacts have major contributions (23% and 22%) due to the relatively high proportion of fluorine and nitrogen atoms interacting in the crystal structure. Moreover, related chromones with $–CF_3$, $–CF_2H$ moieties revealed a high proportion of weak F···H contacts that provide stability to the crystal structures [3,25]. On the other hand, labels 3 and 5 show H···H and C···C contacts with lower percentages of relative contri-

bution (14% and 9%, respectively), related to π···π and C–H···π arrangements. Moreover, a moderate percentage of O···H (10%) hydrogen bonds, due to the oxygen atom of the carbonyl group and hydrogen of benzene moiety [30], is observed. A similar percentage of relative contribution was evidenced for N···F (8%) and C···O (6%) contacts with labels 6 and 7, whose characters will be discussed later through AIM and NCI analysis.

### *2.6. AIM and NCI Analysis of Intermolecular Contacts of* **4**

Figure 5 shows the self-assembled tetramer of compound **4**, where the theory of atoms in molecules (AIM) has been included by visualization of the noncovalent interactions (NCI) by means of the critical points (CPs) and bond paths [34]. Seven CPs were taken into account in order to understand and reveal the weak interactions, where the reduced density gradient (RDG) [35] is visualized with a color. Isosurfaces of the H-bond and halogen bond (blue color), van der Waals interactions (green color) and strong repulsion areas (red color) are shown. In this sense, the seven CPs (1–7) illustrate vdW interactions, where the azide group and their three nitrogen atoms play a significant role, with large RDG isosurfaces (green color), and participate in several N···H and N···F contacts [36]. On the other hand, the combined AIM/NCI plot and topological parameters (Table 4) were calculated using the Multiwfn program [37], considering the main (3, −1) CPs according to Bader´s theory of AIM [34]. Therefore, the topological criteria of electron density [$\rho(r)$] and Laplacian of the electron density $\left[\nabla^2\rho\right]$ showed values that suggest a weak interaction [$\rho(r)$ : 0.0035 − 0.0067; $\nabla^2\rho$: 0.0151 − 0.0295], according to what is proposed by Koch and Popelier [38] to provide information on the nature of interactions. Likewise, the above-mentioned findings are in agreement with Rozas et al. [39], who state that the strength of the hydrogen bond could be evaluated by the sign of $\left[\nabla^2\rho\right]$ and $H(r)$ as total electronic energy density, where weak interactions show values of $\left[\nabla^2\rho\right]$ and $H(r) > 0$ (energy interaction < 12.0 kcal/mol). Moreover, according to Espinosa et al. [40], the $\left|\frac{-V(r)}{G(r)}\right|$ indicator suggests, for all intermolecular contacts, a weak closed-shell (CS) interatomic interaction, according to the values of Table 4 $\left(\left|\frac{-V(r)}{G(r)}\right| < 1 \; and \; Hr > 0\right)$.

**Table 4.** Topological parameters for intermolecular contacts and their (3, −1) CPs [a] for **4**.

| Interaction | CP | $R_{ji}$ | $\rho(r)$ | $\nabla^2\rho$ | $V(r)$ | $G(r)$ | $H(r)$ | $\left\|\frac{-V(r)}{G(r)}\right\|$ |
|---|---|---|---|---|---|---|---|---|
| C7–H7···F2 | CP1 | 2.540 | 0.0058 | 0.0231 | 0.0037 | 0.0048 | 0.0010 | 0.77 |
| C3′–H3′A···F2 | CP2 | 2.669 | 0.0067 | 0.0295 | 0.0048 | 0.0061 | 0.0013 | 0.79 |
| C8–H8···F1 | CP3 | 2.731 | 0.0035 | 0.0151 | 0.0024 | 0.0031 | 0.0007 | 0.77 |
| C2′–H···O2 | CP4 | 2.724 | 0.0043 | 0.0156 | 0.0025 | 0.0032 | 0.0007 | 0.78 |
| C5–H5···N1 | CP5 | 2.779 | 0.0056 | 0.0165 | 0.0029 | 0.0035 | 0.0006 | 0.83 |
| C2′–F1···N2 | CP6 | 3.076 | 0.0058 | 0.0247 | 0.0041 | 0.0052 | 0.0010 | 0.79 |
| C2′–F2···N3 | CP7 | 3.083 | 0.0057 | 0.0236 | 0.0040 | 0.0049 | 0.0010 | 0.81 |

[a] Definitions: $R_{ij}$, bond path (Å); ρ(r), electron density (e Å$^{-3}$); $\nabla^2$ ρ(r), Laplacian of electron density (e Å$^{-5}$); V(r), potential electron density (kJ mol$^{-1}$ br$^{-3}$); G(r), kinetic electron density (kJ mol$^{-1}$ br$^{-3}$); H(r), total electronic energy density (kJ mol$^{-1}$ br$^{-3}$).

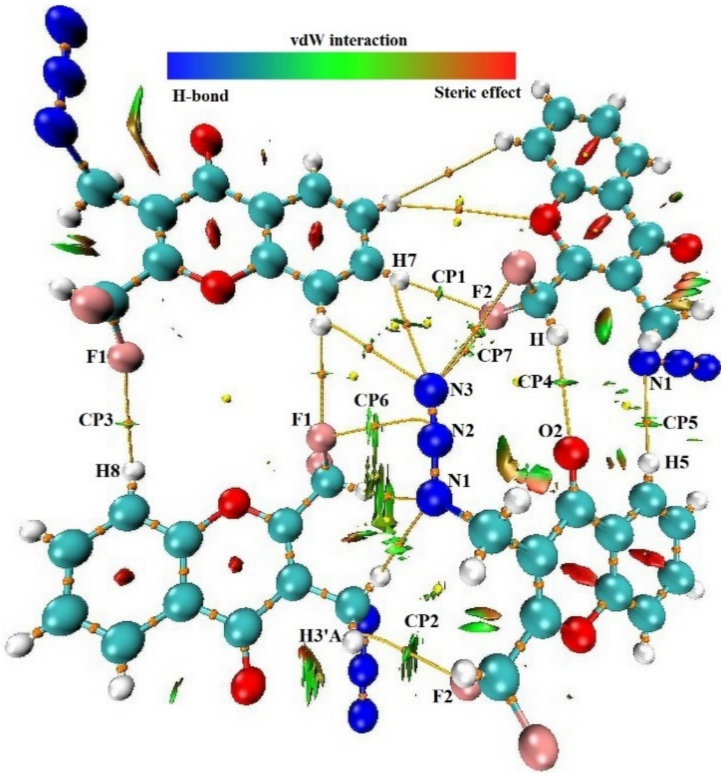


**Figure 5.** Combined AIM/NCI plot analysis of **4**'s tetramer. The bond's critical points (CPs) are represented as yellow spheres with CP labels. For NCI plot, the RDG isosurface is 0.5 and the color range is −0.035–0.02.

## 3. Experimental

### *3.1. General*

All solvents and reagents were from Aldrich (St. Louis, MO, USA) and used without further purification. The melting points (uncorrected) were determined on a Büchi Melting Point M-560 (Büchi Labortechnik AG, Flawil, Switzerland). Infrared absorption spectra (KBr disk) were recorded on Varian 660-IR FT-IR (Agilent Technologies, Santa Clara, CA, USA) spectrometer with 2 $cm^{-1}$ of resolution in the range of 4000–400 $cm^{-1}$ (see Figure S15a, Supplementary Materials). The Raman spectra of the solid were performed in the range of 3500–100 $cm^{-1}$ at room temperature on a Thermoscientific DXR Raman microscope (Thermo Scientific, Madison, WI, USA) using a diode-pumped solid-state laser of 780 nm, with spectral resolution of 5 $cm^{-1}$ (see Figure S15b, Supplementary Materials). The $^{1}$H-, $^{19}$F- and $^{13}$C-NMR spectra were recorded at 25 °C on a Bruker Avance II 500 spectrometer (Bruker, Billerica, MA, USA) using $CDCl_3$ and $CD_3OD$ as solvent. Chemical shifts (δ) are expressed in ppm relative to TMS for $^{1}$H- and $^{13}$C-NMR and TFA (δ = −71.0 ppm) for $^{19}$F-NMR (see Figures S16–S20, Supplementary Materials). Absorbance was measured on a Varian 50 BIO UV-Visible Spectrophotometer (Agilent Technologies, Santa Clara, CA, USA) at 2.0 nm spectral bandwidth using methanol as solvent (see Figures S6–S10, Supplementary Materials). GC-MS spectrometry for 1–3 and 5 were obtained using an Agilent Technologies 7890A chromatograph an 5975C mass-selective detector. The electron energy was 70 eV with a mass range of 50–500 amu and a pressure in the mass spectrometer lower then $10^{-5}$ Torr. The mass spectra are shown in Figures S21–S25 (Supplementary Materials). Mass spectrum of 2 was obtained with a LC-ESI-MS spectrometer UHPLC-MS/MS (model XEVO TQ-S, Waters, Milford, MA, USA) with an electrospray (ESI) interface operating in the positive mode. Reactions were monitored by TLC on silica gel using ethyl acetate/hexane mixtures as a solvent and compounds visualized by UV lamp. The reported yields are for the purified material and are not optimized.

### 3.2. Synthesis: General Procedure for Azidochromones (*1*–*5*)

All bromine-substituted 3-polyhaloalkylchromones were prepared and purified by the reported methods [4,5].

The bromine-substituted 3-polyhaloalkylchromone (0.33 mmol), sodium azide (1.26 mmol) and acetone (10 mL) were added to a 50 mL bottom flask with ground glass joint (Scheme 2). The reaction conditions for each compound are described in the Table S1 (Supplementary Materials). The end of reaction was monitored by TLC (hexane-EtOAc, 9:1). The mixture was filtered and washed with cold acetone, then crude product was dried under vacuum using a rotary evaporator and recrystallized in hexane to yield the pure compound.

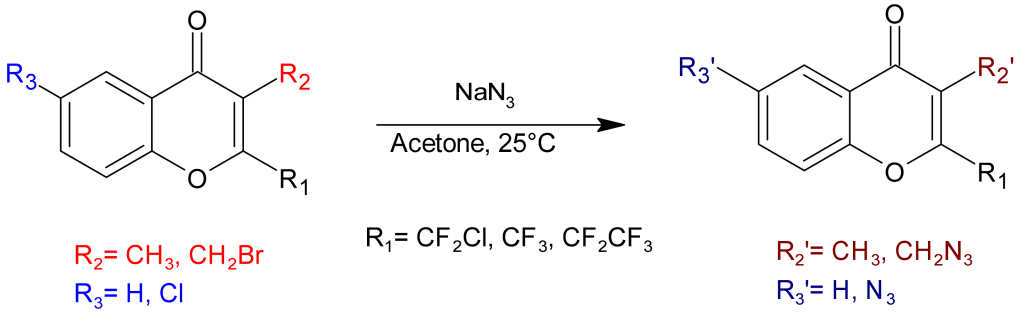


**Scheme 2.** Synthesis of azidochromones **1**–**5**.

*3-Azidomethyl-2-chloro(difluoro)methylchromone* (**1**). White crystalline solid; yield 97%; mp: 70.5–73.6 °C; UV (MeOH): 204, 225, 244, 303 nm; IR (KBr): 2172, 1649, 1609, 1104, 627 $cm^{-1}$; Raman: 2123, 1650, 1609, 671 $cm^{-1}$; $^{1}$H-NMR (500 MHz, $CDCl_3$) δ: 8. 27 (d, *J* = 8 Hz, 1H, H-5), 7.82 (t, *J* = 8.5 Hz, 1H, H-7), 7.59 (d, *J* = 8.5 Hz, 1H, H-8), 7.53 (t, *J* = 8 Hz, 1H, H-6), 4.53 (t, $^{5}J_{H,F}$ = 2 Hz, 2H, $CH_2N_3$); $^{13}$C-NMR (126 MHz, $CDCl_3$) δ: 177.1 (C-4), 154.9 (C-8a), 154,5 (t, $^{2}J_{C,F}$ = 31.3 Hz, C-2) 135.3 (C-7), 126.6 (C-5), 126.3 (C-6), 122.6 (C-4a), 120.8 (t, $^{1}J_{C,F}$ = 292.5 Hz, $CF_2Cl$), 118.4 (C-3), 116.8 (C-8), 42.8 (t, $^{4}J_{C,F}$ = 4.5 Hz, $CH_2N_3$); $^{19}$F-NMR (471 MHz, $CDCl_3$) δ: −54.3 ($CF_2Cl$); GC-MS, 70 eV, *m*/*z*, (rel. int.): 257 (7) $[M - N_2]^+$, 243 (4) $[M - N]^+$, 230 (28) $[M - HCN]^+$, 221 (100) $[M - Cl]^+$.

*6-Azido-3-methyl-2-trifluoromethylchromone* (**2**). White crystalline solid; yield 89%; mp: 72.5–75.5 °C; UV (MeOH): 203, 230, 318 nm; IR (KBr): 2133, 1649, 1605, 1128 $cm^{-1}$; Raman: 2947, 1650, 1606, 1125 $cm^{-1}$; $^{1}$H-NMR (500MHz, $CDCl_3$) δ: 8.19 (d, *J* = 2.5 Hz, 1H, H-5), 7.69 (d, *J* = 9, 2.5 Hz, 1H, H-7), 7.49 (d, *J* = 8.5 Hz, 1H, H-8), 2.25 (q, $^{5}J_{H,F}$ = 2,5 Hz, 3H, $CH_3$); $^{13}$C-NMR (126 MHz, $CDCl_3$) δ: 176.81 (C-4), 153.3 (C-8a), 148.5 (s, $^{2}J_{C,F}$ = 37.2 Hz, C-2), 136.0 (C-6), 134.9 (C-3), 131,9 (C-4a), 125.4 (C-7), 123.2 (C-8), 120.9 (t, C-2′, $^{1}J_{C,F}$ = 280.0 Hz, $CF_3$); 119.9 (C-5), 8.7 (q, $CH_3$, $^{4}J_{C,F}$ = 4.7 Hz); $^{19}$F-NMR (471 MHz, $CDCl_3$) δ: -65.3 ($CF_3$); LC-ESI-MS: $[M - H]^+$ = 270.834 (calculated: 270.048)

*3-Azidomethyl-2-trifluoromethylchromone* (**3**). White crystalline solid; yield 56%; mp: 80–81 °C; UV (MeOH): 204, 223, 250, 305 nm; IR (KBr): 2104, 1653, 1611, 1166, 897 $cm^{-1}$; Raman: 2107, 1647, 1145, 897 $cm^{-1}$; $^{1}$H-NMR (300 MHz, $CDCl_3$) δ: 8.25 (dd, *J* = 8 and 1.5 Hz, 1H, H-5), 7.79 (ddd, *J* = 8.5, 7 and 1.5 Hz, 1H, H-7), 7.55 (d, *J* = 8.5 Hz, 1H, H-8), 7.50 (ddd, *J* = 8, 7 and 1 Hz, 1H, H-6), 4.46 (q, $^{5}J_{H,F}$ = 1 Hz, 2H, $CH_2$); $^{13}$C-NMR (75 MHz, $CDCl_3$) δ: 176.9 (C-4), 155.2 (C-8a), 151.0 (q, $^{2}J_{C,F}$ = 37.7 Hz, C-2), 135.5 (C-7), 126.8 (C-6), 126.4 (C-5), 122.9 (C-4a), 119.4 (q, $^{1}J_{C,F}$ = 277 Hz, $CF_3$), 119.0 (q, $^{3}J_{C,F}$ = 1 Hz, C-3), 118.5 (C-8), 42.8 (q, $^{4}J_{C,F}$ = 2 Hz); $^{19}$F-NMR (282 MHz, $CDCl_3$) δ: -64.5 ($CF_3$); GC-MS, 70 eV, *m*/*z*, (rel. int.): 241 (10) $[M - N_2]^+$, 240 (13) $[M - H]^+$, 227 (6) $[M - N]^+$, 214 (100) $[M - HCN]^+$.

*3-Azidomethyl-2-difluoromethylchromone* (**4**). White crystalline solid; yield 70%; mp: 97.5–99.4 °C; UV(MeOH): 204, 224, 246, 301 nm; IR (KBr): 2094, 1657, 1632, 1107, 900 $cm^{-1}$; Raman: 2105, 1659, 1642, 1112, 903 $cm^{-1}$; $^{1}$H-NMR (600 MHz, $CD_3OD$) δ: 8.18 (d, *J* = 8.1 Hz, 1H, H-5); 7.87 (t, *J* = 7.9 Hz, 1H, H-7); 7.66 (d, *J* = 8.5 Hz, 1H, H-8); 7.55 (t, *J* = 7.5 Hz, 1H, H-6); 7.09 (t, $^{2}J_{H,F}$ = 51.7 Hz, 1H, $CF_2H$); 4.50 (s, 2H, $CH_2N_3$); $^{13}$C-NMR (151 MHz, $CD_3OD$) δ: 178.8 (C-4); 157.2 (t, $^{2}J_{C,F}$ = 24.5 Hz, C-2); 157.0 (C-8a); 136.6 (C-7); 127.5 (C-5); 126,7 (C-6); 124.0 (C-4a); 119.8 (t, $^{3}J_{C,F}$ = 3.2 Hz, C-3); 119.6 (C-8); 111.0 (t, $^{1}J_{C,F}$ = 241.4 Hz, $CF_2H$); 43.3

($CH_2N_3$); $^{19}$F-NMR (565 MHz, $CD_3OD$) δ: −121.99 ($CF_2H$); GC-MS, 70 eV, *m*/*z*, (rel. int.): 223 (38) $[M - N_2]^+$, 209 (14) $[M - N]^+$, 203 (100) $[M - HF]^+$, 196 (93) $[M - HCN]^+$.

*3-Azidomethyl-2-pentafluoroethylchromone* (**5**). Yellow oil at room temperature; yield 28%; UV (MeOH): 204, 221, 246, 304 nm; IR (KBr) 2098, 1659, 1632, 1212, 549 $cm^{-1}$; Raman: 2095, 1657, 1637, 1193, 547 $cm^{-1}$; $^1$H-NMR (600 MHz, $CDCl_3$) δ: 8.26 (dd, *J* = 8 and 1.5 Hz, 1H, H-5); 7.80 (ddd, *J* = 8.5, 7.0 and 1,5 Hz, 1H, H-7); 7.56–7.50 (m, 2H, H-6 and H-8); 4.46 (t, $^5J_{H,F}$ = 2.1 Hz, 2H, $CH_2N_3$); $^{13}$C-NMR (151 MHz, $CDCl_3$) δ: 176,8 (C-4); 155,4 (C-8a); 150,5 (t, $^2J_{C,F}$ = 27,80 Hz, C-2); 135,4 (C-7); 126,9 (C-5); 126,5 (C-6); 122,8 (C-4a); 121,5 (C-3); 118,4 (C-8); 29,9 ($CH_2N_3$); $^{19}$F-NMR (565 MHz, $CDCl_3$) δ: −83.8 (t, *J* = 2 Hz, 3F, $CF_2CF_3$); −116.1 (q, *J* = 2 Hz, 2F, $CF_2CF_3$); GC-MS, 70 eV, *m*/*z*, (rel. int.): 291 (10) $[M - N_2]^+$, 277 (7) $[M - N]^+$, 264 (100) $[M - HCN]^+$.

### *3.3. X ray Diffraction Date and Structural Refinement of* ***4***

The measurements were performed on an Oxford Xcalibur, Gemini, Eos CCD diffractometer (Agilent Technologies XRD Products, Yarnton, UK) with graphite-monochromated MoKα (λ = 0.71073 Å) radiation. X-ray diffraction intensities were collected (ω scans with ϑ and κ-offsets), integrated and scaled with CrysAlisPro [41] suite of programs. The unit-cell parameters were obtained by least-squares refinement (based on the angular setting for all collected reflections with intensities larger than seven times the standard deviation of measurement errors) using CrysAlisPro. Data were corrected empirically for absorption employing the multi-scan method implemented in CrysAlisPro. The non-H structures were solved by the intrinsic phasing procedure implemented in SHELXT [42] and the molecular model refined by full-matrix least-squares with SHELXL of the SHELX suite of programs [43]. The hydrogen atoms were determined in a Fourier difference map phased on the heavier atoms and refined at their found positions with isotropic displacement parameters. Crystal data and structure refinement results are summarized in Table S2 (Supplementary Material). Crystallographic structural data have been deposited at the Cambridge Crystallographic Data Centre (CCDC, Cambridge, UK). Any request to the Cambridge Crystallographic Data Centre for this material should quote the full literature citation and the reference number CCDC 2119625.

### *3.4. Computational Details*

Quantum chemical calculations were performed for the ground state (gas phase) of **1**–**5** with the Gaussian 09 [44]. Scans of the potential energy surface were carried out with the B3LYP/6-311++G(d,p) level of theory. Potential energy curves were performed around the dihedral angles involving the nitrogen, chlorine and fluorine atoms (C3C2-C2′F, C4C3-C3′N, C2C3-C3′N and C2C3-C3′Cl) (see Figures S1–S4, Supplementary Materials).

The geometry optimizations calculations were carried out with the Density Functional Theory (B3LYP) method, employing the 6-311++G(d,p) basis set. In all cases, the calculated vibrational properties correspond to potential energy minima with no imaginary values for the frequencies. The $^1$H- and $^{13}$C- chemical shifts were calculated for the optimized geometries (B3LYP/6-311+G(2d,p)) using the GIAO method (Gauge Including Atomic Orbital), with the corresponding TMS shielding calculated at the same level of theory. The electronic transitions were calculated with the Time-Dependent Density Functional Theory (TD-DFT), implicitly considering the solvent effect (methanol).

### *3.5. Hirshfeld Surface Calculations of* ***4***

The 2D-fingerprint plots of the Hirshfeld surface, energy frameworks and lattice interaction energies of **4** were generated using CrystalExplorer v17.5 software [45]. The incidence of each intermolecular interaction in the crystal was visualized and decoded from the 2D-fingerprint plot. The normalized contact distance surface ($d_{norm}$) based on $d_i$ and $d_e$, (contact distances normalized by the van der Waals (vdW) radii) can be visualized by red spots, the 3D $d_{norm}$ surfaces are mapped over a fixed color scale of −0.243 au (red)–0.824 Å au (blue), shape index in the color range of −1.0 au (concave)–1.0 au (convex)

Å and curvedness index in the range of 14−4.0 au (flat)–0.4 au (singular) Å. The surface properties mentioned above ($d_{norm}$, shape and curvedness index) were used to identify planar stacking. Moreover, the intermolecular interaction energies of (**4**) were calculated using TONTO program, integrated in the CrystalExplorer v17.5 software. The interaction energies (Table S8 and Figure S26, Supplementary Materials) between the molecules are obtained using CE-B3LYP model (B3LYP/6-31G(d,p)).

## 4. Conclusions

Five azidochromones were fully characterized by NMR ($^{1}$H-, $^{13}$C-, $^{19}$F-) and electronic (UV-Vis) spectroscopies and GC-MS and UHPLC-MS/MS spectrometric methods. From the most stable conformations (theoretical calculations) for each of the compounds, the NMR and electronic spectra were simulated to aid the interpretation and compare these data with experimental results. A good accordance was found between experimental and calculated spectra. The crystal packing of 4 showed weak intermolecular interactions that promote the stabilization of the supramolecular assembly. Therefore, theoretical approaches such as Hirshfeld surface, AIM and NCI analysis were useful to understand the relative contributions of contacts and the character of weak intermolecular interactions in the context of electronic density. The analysis revealed that the F···H (23%), N···H (22%) and O···H (10%) contacts associated to $–CF_2H$, $–N_3$ and –C=O groups and H···H (14%), C···C (9%) contacts associated with π···π stacking and C–O···π interactions are the main driving forces in crystal-packing formation. Moreover, the topological parameters studied by NCI/AIM methods evidenced a significant role of the azide (–N=N=N) group contributing through three nitrogen atoms to several bond-critical points. In addition, the reduced density gradient (RDG) characterized the weak intermolecular interactions as van der Waals interactions, where the electronic density can be considered as weak closed-shell (CS) interatomic interactions.

**Supplementary Materials:** The following supporting information are available online. Scheme S1. General procedure of the synthesis of novel azidochromones, Figure S1. Potential energy curve for 1, Figure S2. Potential energy curve for 2, Figure S3. Potential energy curve for 3, Figure S4. Potential energy curve for 5, Figure S5. Linear relationship data $^{1}$H-NMR 1–5, Figure S6. Experimental and calculated UV-Vis spectra of 1, Figure S7. Experimental and calculated UV-Vis spectra of 2, Figure S8. Experimental and calculated UV-Vis spectra of 3, Figure S9. Experimental and calculated UV-Vis spectra of 4, Figure S10. Experimental and calculated UV-Vis spectra of 5, Figure S11. Molecular orbitals involved in the electronic transitions of 1 and 2. The energy scale is only qualitative, Figure S12. Molecular orbitals involved in the electronic transitions of 3 and 4. The energy scale is only qualitative, Figure S13. Molecular orbitals involved in the electronic transitions of 5. The energy scale is only qualitative, Figure S14. Interaction energies for 4, Figure S15. (a) IR and (b) Raman spectra of 1–5, Figure S16. Compound 1 (a) $^{1}$H-NMR, (b) $^{13}$C-NMR and (c) $^{19}$F-NMR, Figure S17. Compound 2 (a) $^{1}$H-NMR, (b) $^{13}$C-NMR and (c) $^{19}$F-NMR, Figure S18. Compound 3 (a) $^{1}$H-NMR, (b) $^{13}$C-NMR and (c) $^{19}$F-NMR, Figure S20. Compound 5 (a) $^{1}$H-NMR, (b) $^{13}$C-NMR and (c) $^{19}$F-NMR, Figure S21. GS-MS of 1, Figure S22. HPLC-EM of 2, Figure S23. GS-MS of 3, Figure S24. GS-MS of 4, Figure S25. GS-MS of 5, Figure S26. Crystal lattice energy analysis applying the CE-B3LYP/6-31G(d,p) energy model and figures of energy frameworks for 4. (a) Total Energy (b) Electrostatic Energy, (c) Dispersive Energy, Table S1. Reaction conditions for 1 – 5 compounds, Table S2. Crystal data and structure refinement results for 3-dibromomethyl-2-difluoromethyl chromone, Table S3. Bond lengths [Å] and angles [°] for 3-azidomethyl-2-difluoromethyl chromone (4), Table S4. Angles [°] for 3-azidomethyl-2-difluoromethyl chromone (4), Table S5. Fractional Atomic Coordinates ($\times 10^4$) and Equivalent Isotropic displacement Parameters ($Å^2 \times 10^3$) for 4. $U_{eq}$ is defined as 1/3 of the trace of the orthogonalized $U_{IJ}$ tensor, Table S6. Selected intermolecular contacts [Å and °] for 4, Table S7. Geometrical parameters for the π-stacking moieties involved in the π···π interactions of 4 (Å, º), Table S8. Geometrical parameters of C-O···π interactions* for 4 (Å, º), Table S9. Interaction energies (kJ/mol) for 4, Table S10. Scale factors for benchmarked energy models.

**Author Contributions:** Conceptualization, C.D.A.-L., S.E.U., J.L.J. and P.L.; Data curation, J.H.-M. and O.E.P.; Formal analysis, D.A.Z.-S., C.D.A.-L., L.A.R.-G., S.E.U., J.L.J. and O.E.P.; Investigation,

E.G.N.-O., K.A.P.-C., P.M.B.-V., T.G.Y.-D., C.D.A.-L., J.H.-M., S.E.U., J.L.J. and P.L.; Methodology, K.A.P.-C., C.D.A.-L., S.E.U. and J.L.J.; Validation, C.D.A.-L.; Writing—original draft, E.G.N.-O., D.A.Z.-S., P.M.B.-V., T.G.Y.-D., C.D.A.-L., J.H.-M., L.A.R.-G., S.E.U., J.L.J., O.EP., G.A.E. and P.L.; Writing—review and editing, D.A.Z.-S. All authors have read and agreed to the published version of the manuscript.

**Funding:** The work was supported by Central University of Ecuador (Grant, DI-CON-2019-007), Faculty of Chemical Sciences, and CONICET (Grant PIP 0651) and UNLP (Grant 11/X857) of Argentina.

**Institutional Review Board Statement:** Not applicable.

**Informed Consent Statement:** Not applicable.

**Data Availability Statement:** All data generated or analysed during this study are included in this published article [and its additional information file].

**Acknowledgments:** We thank Silvana Díaz and Alexander Medina of Laboratorio de Contaminantes—AGROCALIDAD—Ecuador for their contribution in the experimental determination of **2** by HPLC-MS. S.E.U., G.A.E. and O.E.P. are research fellows of CONICET-Argentina and J.L.J. is research fellow of CICPBA-Argentina.

**Conflicts of Interest:** The authors declare no conflict of interest.

**Sample Availability:** Samples of the compounds are available from the authors.

## References

1. Sosnovskikh, V.Y. Synthesis and Reactions of Halogen-Containing Chromones. *Russ. Chem. Rev.* **2003**, *72*, 489–516. [CrossRef]
2. Sosnovskikh, V.Y.; Korotaev, V.Y.; Chizhov, D.L.; Kutyashev, I.B.; Yachevskii, D.S.; Kazheva, O.N.; Dyachenko, O.A.; Charushin, V.N. Reaction of Polyhaloalkyl-Substituted Chromones, Pyrones, and Furanones with Salicylaldehydes as a Direct Route to Fused 2H-Chromenes. *J. Org. Chem.* **2006**, *71*, 4538–4543. [CrossRef] [PubMed]
3. Alcívar León, C.D.; Echeverría, G.A.; Piro, O.E.; Ulic, S.E.; Jios, J.L.; Pereañez, J.A.; Henao Castañeda, I.C.; Pérez, H. The Role of Non-Covalent Interactions in Some 2-Trifluoromethylchromones in the Solid State. *New J. Chem.* **2017**, *41*, 14659–14674. [CrossRef]
4. Alcívar León, C.D. Estudio de Nuevos Benzopiranos Haloalquil Sustituidos. PhD Thesis, Universidad Nacional de La Plata, La Plata, Argentina, 2016.
5. Narváez, O.E.G.; Bonilla, V.P.M.; Zurita, D.A.; Alcívar, L.C.D.; Heredia-Moya, J.; Ulic, S.E.; Jios, J.L.; Piro, O.E.; Echeverría, G.A.; Langer, P. Synthesis, Experimental and Theoretical Study of Novel 2-Haloalkyl (-CF2H, -CCl2H, -CF2CF3)-, 3-Bromo and Bromomethyl Substituted Chromones. *J. Fluor. Chem.* **2021**, *242*, 109717. [CrossRef]
6. Gomes, A.; Neuwirth, O.; Freitas, M.; Couto, D.; Ribeiro, D.; Figueiredo, A.G.P.R.; Silva, A.M.S.; Seixas, R.S.G.R.; Pinto, D.C.G.A.; Tomé, A.C.; et al. Synthesis and Antioxidant Properties of New Chromone Derivatives. *Bioorg. Med. Chem.* **2009**, *17*, 7218–7226. [CrossRef]
7. Fitton, A.O.; Hatton, B.T. Pharmacologically Active 4-Oxo-4H-Chromen-2-Carboxylic Acids. Part II. The Synthesis of 4-Oxo-4H-Chromen-2-Carboxylic Acids Containing a Fused Imidazole or Oxazole Ring. *J. Chem. Soc. C Org.* **1970**, 2518–2522. [CrossRef]
8. Chohan, M.I.; Fitton, A.O.; Hatton, B.T.; Suschitzky, H. Pharmacologically Active 4-Oxo-4H-Chromen-2-Carboxylic Acids. Part III. Mechanistic Aspects of the Decomposition of Ethyl 6-Azido-4-Oxo-4H-Chromen-2-Carboxylate. *J. Chem. Soc. C Org.* **1971**, 3079–3081. [CrossRef]
9. Tome, S.M.; Tome, A.C.; Soengas, R.G.; Silva, A.M.S. Chalcones and Chromones in Copper-Catalyzed Azide–Alkyne Cycloadditions (CuAAC). *Curr. Org. Chem.* **2018**, *22*, 1307–1325. [CrossRef]
10. Machado, N.F.L.; Marques, M.P.M. Bioactive Chromone Derivatives—Structural Diversity. *Curr. Bioact. Compd.* **2010**, *6*, 76–89. [CrossRef]
11. Ellis, G.P. Chromones. In *Chemistry of Heterocyclic Compounds: Chromenes, Chromanones, and Chromones*; John Wiley & Sons, Inc.: Toronto, ON, Canada, 1977; Volume 31, p. 613. ISBN 0-471-38212-4.
12. Sharma, S.; Kumar, S.; Chand, K.; Kathuria, A.; Gupta, A.; Jain, R. An Update on Natural Occurrence and Biological Activity of Chromones. *Curr. Med. Chem.* **2011**, *18*, 3825–3852. [CrossRef]
13. Khadem, S.; Marles, R.J. Chromone and Flavonoid Alkaloids: Occurrence and Bioactivity. *Mol. Basel Switz.* **2011**, *17*, 191–206. [CrossRef] [PubMed]
14. Tome, S.M.; Silva, A.M.S.; Santos, C.M.M. Synthesis and Transformation of Halochromones. *Curr. Org. Synth.* **2014**, *11*, 317–341. [CrossRef]
15. Bräse, S.; Banert, K. Lab—Scale Synthesis of Azido Compounds: Safety Measures and Analysis. In *Organic Azides: Syntheses and Applications*; Wiley: Chichester, UK, 2010; pp. 3–4. ISBN 9780470519981.
16. Wen, L.; Zhang, H.; Lin, H.; Shen, Q.; Lu, L. A Facile Synthetic Route to 2-Trifluoromethyl-Substituted Polyfunctionalized Chromenes and Chromones. *J. Fluor. Chem.* **2012**, *133*, 171–177. [CrossRef]

17. Sosnovskikh, V.Y.; Irgashev, R.A.; Usachev, B.I. Synthesis and Some Properties of 2-(Polyfluoroalkyl)Chroman-4-Ols and 2-(Polyfluoroalkyl)Chroman-4-Ones. *Russ. Chem. Bull.* **2009**, *58*, 2465–2473. [CrossRef]
18. Chang, M.-Y.; Tsai, Y.-L. Stereocontrolled Synthesis of 3-Sulfonyl Chroman-4-Ols. *J. Org. Chem.* **2018**, *83*, 6798–6804. [CrossRef]
19. Malets, Y.S.; Moskvina, V.S.; Grygorenko, O.O.; Brovarets, V.S. Synthesis of Azachromones and Azachromanones. *Chem. Heterocycl. Compd.* **2019**, *55*, 1007–1012. [CrossRef]
20. Duan, Y.; Jiang, Y.; Guo, F.; Chen, L.; Xu, L.; Zhang, W.; Liu, B. The Antitumor Activity of Naturally Occurring Chromones: A Review. *Fitoterapia* **2019**, *135*, 114–129. [CrossRef]
21. Patil, V.M.; Masand, N.; Verma, S.; Masand, V. Chromones: Privileged Scaffold in Anticancer Drug Discovery. *Chem. Biol. Drug Des.* **2021**, *98*, 943–953. [CrossRef]
22. Benny, A.T.; Arikkatt, S.D.; Vazhappilly, C.G.; Kannadasan, S.; Thomas, R.; Leelabaiamma, M.S.N.; Radhakrishnan, E.K.; Shanmugam, P. Chromone a Privileged Scaffold in Drug Discovery: Developments on the Synthesis and Bioactivity. *Mini Rev. Med. Chem.* **2021**. [CrossRef]
23. Sosnovskikh, V.Y. Fluorinated Pyrones, Chromones and Coumarins BT—Fluorine in Heterocyclic Chemistry. In *6-Membered Heterocycles*; Nenajdenko, V., Ed.; Springer International Publishing: Cham, Switzerland, 2014; Volume 2, pp. 211–290. ISBN 978-3-319-04435-4.
24. Alcívar León, C.D.; Echeverría, G.A.; Piro, O.E.; Ulic, S.E.; Jios, J.L.; Burgos Paci, M.; Argüello, G.A. The Role of Halogen C–X1···X2–C Contact on the Preferred Conformation of 2-Perhalomethylchromones in Solid State. *Chem. Phys.* **2016**, *472*, 142–155. [CrossRef]
25. Alcívar León, C.D.; Ramos Guerrero, L.A.; Bonilla Valladares, P.M.; Echeverría, G.A.; Piro, O.E.; Ulic, S.E.; Jios, J.L.; Langer, P. Synthesis and Structural Study of 2-(Haloalkyl)-3-Methylchromones. *Mon. Für Chem. Chem. Mon.* **2019**, *150*, 1929–1940. [CrossRef]
26. Alcívar León, C.D.; Piro, O.E.; Echeverria, G.A.; Ulic, S.E.; Jios, J.L. Synthesis and Conformational Theoretical Study of Novel Derivatives of 2-(Trifluoromethyl)Chromone: 3-Cyanomethyl and 3-Aminomethyl 2-(Trifluoromethyl)Chromones. *J. Argent. Chem. Soc.* **2014**, *101*, 1207–1852.
27. Alcívar León, C.D.; Echeverría, G.A.; Piro, O.E.; Ulic, S.E.; Jios, J.L. A Detailed Experimental and Theoretical Study of Two Novel Substituted Trifluoromethylchromones. The Influence of the Bulky Bromine Atom on the Crystal Packing. Spectrochim. *Acta Part Mol. Biomol. Spectrosc.* **2015**, *136*, 1358–1370. [CrossRef] [PubMed]
28. Farrugia, L. ORTEP-3 for Windows—A Version of ORTEP-III with a Graphical User Interface (GUI). *J. Appl. Crystallogr.* **1997**, *30*, 565. [CrossRef]
29. Batsanov, A. Weak Interactions in Crystals: Old Concepts, New Developments. *Acta Crystallogr. Sect. E Crystallogr. Commun.* **2018**, *74*, 570–574. [CrossRef]
30. Seth, S.K.; Sarkar, D.; Kar, T. Use of π–π Forces to Steer the Assembly of Chromone Derivatives into Hydrogen Bonded Supramolecular Layers: Crystal Structures and Hirshfeld Surface Analyses. *CrystEngComm* **2011**, *13*, 4528–4535. [CrossRef]
31. Li, P.; Vik, E.C.; Maier, J.M.; Karki, I.; Strickland, S.M.S.; Umana, J.M.; Smith, M.D.; Pellechia, P.J.; Shimizu, K.D. Electrostatically Driven CO−π Aromatic Interactions. *J. Am. Chem. Soc.* **2019**, *141*, 12513–12517. [CrossRef]
32. Spackman, P.; Turner, M.; McKinnon, J.; Wolff, S.; Grimwood, D.; Jayatilaka, D.; Spackman, M. CrystalExplorer: A Program for Hirshfeld Surface Analysis, Visualization and Quantitative Analysis of Molecular Crystals. *J. Appl. Crystallogr.* **2021**, *54*, 1006–1011. [CrossRef]
33. Spackman, M.A.; Jayatilaka, D. Hirshfeld Surface Analysis. *CrystEngComm* **2009**, *11*, 19–32. [CrossRef]
34. Bader, R.F.W. A Quantum Theory of Molecular Structure and Its Applications. *Chem. Rev.* **1991**, *91*, 893–928. [CrossRef]
35. Boto, R.A.; Contreras-García, J.; Tierny, J.; Piquemal, J.-P. Interpretation of the Reduced Density Gradient. *Mol. Phys.* **2016**, *114*, 1406–1414. [CrossRef]
36. Bursch, M.; Kunze, L.; Vibhute, A.M.; Hansen, A.; Sureshan, K.M.; Jones, P.G.; Grimme, S.; Werz, D.B. Quantification of Noncovalent Interactions in Azide–Pnictogen, –Chalcogen, and –Halogen Contacts. *Chem. Eur. J.* **2021**, *27*, 4627–4639. [CrossRef] [PubMed]
37. Lu, T.; Chen, F. Multiwfn: A Multifunctional Wavefunction Analyzer. *J. Comput. Chem.* **2012**, *33*, 580–592. [CrossRef] [PubMed]
38. Koch, U.; Popelier, P.L.A. Characterization of C-H-O Hydrogen Bonds on the Basis of the Charge Density. *J. Phys. Chem.* **1995**, *99*, 9747–9754. [CrossRef]
39. Rozas, I.; Alkorta, I.; Elguero, J. Behavior of Ylides Containing N, O, and C Atoms as Hydrogen Bond Acceptors. *J. Am. Chem. Soc.* **2000**, *122*, 11154–11161. [CrossRef]
40. Espinosa, E.; Alkorta, I.; Elguero, J.; Molins, E. From Weak to Strong Interactions: A Comprehensive Analysis of the Topological and Energetic Properties of the Electron Density Distribution Involving X–H···F–Y Systems. *J. Chem. Phys.* **2002**, *117*, 5529–5542. [CrossRef]
41. *CrysAlisPRO Including ABSPACK 2009*; Oxford Diffraction / Agilent Technologies UK Ltd.: Yarnton, UK, 2009.
42. Sheldrick, G. Crystal Structure Refinement with SHELXL. *Acta Crystallogr. Sect. C* **2015**, *71*, 3–8. [CrossRef]
43. Sheldrick, G. A Short History of SHELX. *Acta Crystallogr. Sect. A* **2008**, *64*, 112–122. [CrossRef]

44. Frisch, M.J.; Trucks, G.W.; Schlegel, H.B.; Scuseria, G.E.; Robb, M.A.; Cheeseman, J.R.; Scalmani, G.; Barone, V.; Petersson, G.A.; Nakatsuji, H.; et al. *Gaussian 09, Revision A.02 2009*; Gaussian, Inc.: Wallingford, CT, USA, 2016.
45. Mackenzie, C.F.; Spackman, P.R.; Jayatilaka, D.; Spackman, M.A. CrystalExplorer Model Energies and Energy Frameworks: Extension to Metal Coordination Compounds, Organic Salts, Solvates and Open-Shell Systems. *IUCrJ* **2017**, *4*, 575–587. [CrossRef]